TEMPERATURE EFFECT ON INTERMOLECULAR STRUCTURE OF LIQUID WATER

by

Mahmood Nilforoushan Nily

Submitted in Partial Fulfillment of the Requirements

for the Degree of

Master of Science

in the

Chemistry Program

(Signature) Howard D. Mettee December 28, 1992
Advisor Date

(Signature) Sally M. Hotchkiss December 28, 1992
Dean of Graduate School Date

YOUNGSTOWN STATE UNIVERSITY

August 1992

Youngstown State University

Graduate School

Thesis

Submitted in partial fulfillment of the requirements for the degree of Master of Science

TEMPERATURE EFFECT ON INTERMOLECULAR STRUCTURE OF LIQUID WATER

Presented by Mahmood Nilforoushan Nily

Accepted by the Department of Chemistry

Howard D. Mettee — December 28, 1992
Major Professor — Date

Daryl W. Kinney — December 28, 1992
Professor — Date

Steven M. Schildcrout — 12/28/92
Professor — Date

Thomas N. Robbelstein — 12-28-92
Chairman, Chemistry Department — Date

Sally M. Hotchkiss — December 28, 1992
Dean, Graduate School — Date

ABSTRACT

TEMPERATURE EFFECT ON INTERMOLECULAR STRUCTURE OF LIQUID WATER

Mahmood Nilforoushan Nily

Master of Science

Youngstown State University, 1992

The temperature dependence of the Fourier Transform Infrared (FTIR) spectra of liquid water (H_2O) and heavy water (D_2O), using total internal reflectance cells with crystals of zinc selenide (ZnSe) and germanium (Ge), is interpreted as a composite of three overlapping bands whose areas reflect the concentrations of forms of water in a dynamic, three-way equilibrium. The overall observation, that the experimental profile shifts intensity from the low frequency (traditionally, more strongly hydrogen-bonded) to the high frequency (more weakly-bonded) sides, is reproduced by the deconvolution program (Bandfit) to within 95% or better in most cases. For the equilibrium A $\rightleftharpoons$ B, B $\rightleftharpoons$ C, and A $\rightleftharpoons$ C (A the most stable, B the less stable, and C the least stable) the ΔH values are 0.98 $\pm$ 0.22, 0.62 $\pm$ 0.28, and 1.57 $\pm$ 0.16 kcal/mol, respectively for water (independent of crystal). The corresponding values for D_2O are 1.37 $\pm$ .0.25, 0.68 $\pm$ 0.30, and 2.07 $\pm$ 0.30 kcal/mol, respectively. Hess's law is obeyed, within experimental error, for both isotopic species, and the ratios of the

corresponding ΔHs for D_2O/H_2O are either unity (B $\rightleftharpoons$ C), or the square root of the mass ratio M_D/M_H (A $\rightleftharpoons$ B and A $\rightleftharpoons$ C), indicating a primary isotope effect.

ACKNOWLEDGEMENTS

I would like to thank Dr. Howard D. Mettee whose guidance and help made this thesis possible.

I would also like to extend my appreciation to Drs. Daryl Mincey and Steven Schildcrout for their time and effort reviewing the manuscript.

TABLE OF CONTENTS

PAGE

LIST OF SYMBOLS

SYMBOL	DEFINITION	UNITS
ΔH	Enthalpy Change	kcal/mol
p	Final Radiant Power	cadl/sr/s
P_o	Initial Radiant Power	" " "
l	Radiation Path Length	cm
c	Concentration	mol/L
k	Bendony Force Constant	J/radian
ν	Frequency	cm-1
Σ	Summation	
T	Transmittance	
ΔS	Entropy Change	J mol-1K-1
R	Gas Constant	J mol-1K-1
ϵ_A	Molar extinction coefficient	
v	Quantum No.	
T	Temperature	Kelvin (K)
U	Potential Energy	J/mol
n	Refractive Index	
θ	Angle of light ray to normal	degrees
$\varnothing$	Distortion angle of H-bond	radius

LIST OF FIGURES

FIGURE PAGE

LIST OF TABLES

CHAPTER I

INTRODUCTION

Liquid Water Structure

For the present purposes, the structure of liquid water may be considered to have two possible models - a continuum model, due to Bernal and Fowler,[1] or a mixture model developed by Pauling.[2] The continuum model assumes each water molecule is in a structureless cavity of surrounding water molecules of continuous (but temperature variant) dielectric constant. The mixture model assumes a series of discrete equilibria between water molecules with different numbers of H-bonds, thereby taking explicit account of the structure of the water molecule.

Some spectroscopic investigations favor a continuum type of model,[1] but others favor a mixture type model.[2]

The infrared absorption spectrum of the fundemental OH vibrational stretching region of water suggests the presence of multiply H-bonded species including a "four-bonded" species, where the water molecule is both a double-donor and double-acceptor of H-bonds.

The fact that the intermolecular intensities are small near 100°C, where the H-bonded intramolecular intensities are large, indicates that a consecutive or

stepwise breakage or disruption of H-bonds may be involved as liquid water is heated.

The basis of the liquid phase of water is related to the near tetrahedral arrangement of the two polar O-H bonds and the two non-bonding electron pairs of the water molecule.[3]

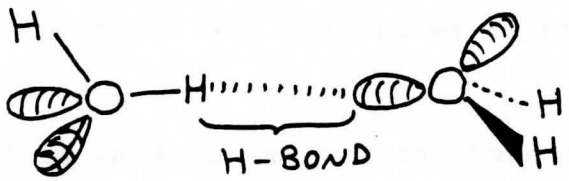

Fig.1 Geometry of H-bond in water dimer (gas phase).[4]

Raman spectroscopic investigation of this problem using band deconiolution techniques date mostly to the mid sixties, after which little progress was reported. These studies used four or more overlapping contributing bands to synthetically reproduce the experimentally observed band profile. The present study uses a maximum of only three bands to represent the experimental profile, which is capable of reducing the residual error to less than 5%.

CHAPTER II

Theory of Hydrogen Bonding

Among the various types of intermolecular interactions, the H-bond plays the most significant role in determining the structure and properties of chemical and biological molecules.

An H-bond is said to exist when there is evidence that this bond specifically involves a hydrogen atom covalently bonded to another atom, say X, which is also attached to an atom in another molecule (Y). Pauling[2] first suggested that in an H-bond, X —— H - - - Y, the hydrogen 1s orbital can form only one covalent bond with X, so the interaction with Y (electron pair donor) is largely electrostatic in character. Several properties of the H-bond have been interpreted on the basis of this essentially electrostatic model, which is largely the view accepted today.[4,5]

Mixture Models

The structure of water at any instant is postulated to be a mixture of a small number of distinguishable species of water molecules, called V-structure. For instance, in one type of V-model, only two species of water molecules are supposed to be present at any given instant.[6]

Molecules are either in "clusters" or monomeric. In clusters, there are H-bonded molecules, whereas the monomeric water is not H-bonded. The molecules in clusters are H-bonded to four neighboring molecules. The clusters are constantly breaking up and re-forming, so that over a long period of time every water molecule has the same average environment; with increasing the concentration of non-H-bonded free molecules increases.[2,8]

Flickering-Cluster Model

The flickering-cluster model suggests that formation of hydrogen bonds in liquid water is a cooperative phenomenon and a pair of H-bonded atoms promote the tendency of each atom to H-bond to another neighbor to form groups of H-bonded water molecule called clusters.[9,10] The result of the cooperative H-bonding is that when one bond forms, there is a tendency for several more to form, and when one breaks, an entire group tends to break. This process produces short-lived, ice-like, flickering clusters of highly H-bonded molecules. These clusters are mixed with non-H-bonded molecules, which form one or two layers between them, and the whole system is held together by van der Waals binding forces.[11,12]

Due to a partially covalent character[13,14] of the hydrogen bond, the remaining lone-pair electrons of oxygen atoms in a H-bonded chain of liquid water molecules are more localized, with more nearly tetrahedral sp^3 hybridization

than if the molecules were not members of the chain.[12] The clusters should be compact, with as many quadruply-bonded molecules as possible and very few extended chains of doubly-bonded molecules. The fulfillment of the condition of a high degree of H-bonding in the flickering-cluster model can occur through a large number of structural networks. The tridymite-like arrangement such as occurs in ice is likely to occur frequently in liquid water, because it involves a relatively large number of H-bonds for a given cluster size.[10]

CHAPTER III

CONTINUUM MODELS

Distorted Hydrogen-Bond Model

Pople[13,14] (1951) developed a model for liquid water in which the majority of H-bonds are regarded as distorted rather than broken. According to this model of liquid water, when ice melts, the flexibility of the hydrogen bonds greatly increases. Rearrangement of water structure with changes in temperature takes place as a result of bending or distortion of most of the H-bonds.[8] Bending of the H-bonds results in continous destruction of the ice lattice leading to irregular arrangement of water molecules. Bending of the H-bonds is regarded as a continuously variable rotation of the hydrogen atom, or the lone-pair electrons, or both, out of the O ... O line of centers.[15]

Pople[14] assumed that all molecules in liquid water are H-bonded to four neighbors and each water molecule is near tetrahedral.

A hydrogen bond is considered undistorted in Pople's[14] model when both the O-H of a donor water molecule and the lone-pair to which it is H-bonded, lie along the oxygen-oxygen line of the two molecules. In other words, the energy of the hydrogen bond bending vanishes when all H_2O---H_2O---H_2O angles are tetrahedral, as

is the case with the most common form of ice.[16] When either the lone-pair directions or the O-H bond directions depart from the oxygen-oxygen line by an angle ϕ, the hydrogen bond is distorted, and the energy of the system is increased by $\delta U = k\phi\,(1-\cos\phi)$, where $k\phi$ is the H-bond bending force constant.[20]

Molecular Vibrations

The nuclei of molecules, with respect to each other, are in a continuous state of vibration, even at zero Kelvin. These vibrations can be described by a limited number of basic vibrations known as normal modes. A normal mode is a vibration in which all the nuclei oscillate with the same frequency. The water molecule has three normal modes, and every possible vibration of the molecule is a superposition of these three modes.[18] The normal modes of vibration of water are shown in Figure 2. Because the motion of nuclei in the ν_1 and ν_3 vibration is along the direction of the O-H bonds, these modes are often referred to as O-H stretching vibrations. Similarly, because the H nuclei in ν_2 move in direction almost perpendicular to the bonds, ν_2 is referred to as the H-O-H bending vibration. The mode ν_3 is called the asymmetric (out-of-phase) stretching vibration, and ν_1 is called the symmetric (in-phase) stretching vibration.[7]

The transition of water molecules from their vibrational ground states to an excited state described by

the ν_2 mode is associated with the infrared absorption band at 1594 cm^{-1}. During this transition, the quantum number V_2 changes from 0 to 1, while the quantum number V_1 for ν_1 and V_3 for ν_3 remain equal to zero.[4] Similarly, the transition

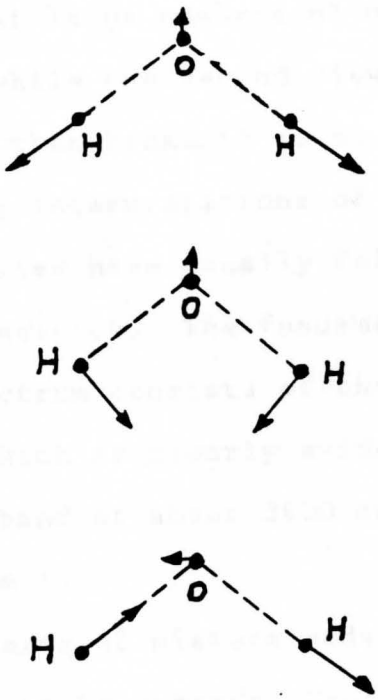

$\nu_1 = 3656.65\ cm^{-1}$

$\nu_2 = 1594.56\ cm^{-1}$

$\nu_3 = 3755.79\ cm^{-1}$

Fig. 2. The normal modes of vibration of H_2O (g). The bonds are represented by dashed lines. The arrows show the relative directions and displacements of the nuclei during a given vibration.[18]

from the ground state to the state in which only the first normal mode is excited, where $V_1 = 1$, $V_2 = 0$, and $V_3 = 0$, is associated with the absorption band at 3656 cm^{-1}.

Vibrational Spectra of Molecules in Liquid Water

There are two principal models of liquid water. One proposes that large numbers of discrete H-bonds exist (Pauling)[2] while the second view considers that H-bonds are bent rather than broken[13] (i.e. the structural continuum of Pople). The interpretations of infrared and Raman spectra of liquid water have usually followed one or the other of the above theories. The fundamental OH stretching region of the H_2O spectrum consists of three bands: a shoulder near 3600 cm^{-1} which is clearly evident in the present spectrum, an intense band at about 3400 cm^{-1}, and another shoulder near 3250 cm^{-1}.

In terms of mixture model, which involves making and breaking discrete H-bonds, Rao[19] assigned these absorptions to vibrations of monomer, dimer and trimer species in liquid water. Burnham and Leighton[20] attributed them to vibrations of zero-, two-, and four-coordinated water molecules. Another interpretation is given in terms of non-bonded, one-bonded, and two-bonded molecules. In terms of a bond-bending[8] approach, most of the waters are considered to be tetra-coordinated molecules and the modified stretching bands are assigned to ν_1, ν_3, and $2\nu_2$ of these molecules.

There is clearly much discrepency in the literature concerning the origin of these bands in the stretching region of liquid water.

Interpretation of OH Stretching Region of Liquid H_2O

Because of the presence of a near-continuum of different types of water molecules, with different degrees of distortions, one would not expect just one ν_1 and one ν_3 band but a continuum of ν_{1d} and ν_{3d} absorption, (where "d" indicates a range of frequencies). These would be essentially H-bonded absorptions with perhaps only a few percent of the total band intensity due to absorptions with strictly ν_1 and ν_3 (free) character.[21]

It is expected that one of the three components of the H-bonded OH stretching fundamental stretching region is due to an overtone of the bending mode ($2\nu_2$). However, it is difficult to make a unique assignment, as Hornig[22] did on the basis of concentrated salt mixture breaking up the H-bonded structure.

Furthermore, the three OH stretching components show temperature effects characteristic of three different OH environments of water molecules in equilibrium. These effects could be interpreted as a change in the perturbing[4] environments on ν_1, ν_3, and $2\nu_2$ of individual water molecules. However, this thesis considers the temperature effects to fit the three-way equilibrium model.[23]

Maxwellian Distribution of Collisions

Each collisional interaction originates from a different type of local environment about the OH group in liquid water. Each different environment leads to a different OH frequency. Different environments originate from the thermal motion of the solution, which perturbs the environment and may be considered a "collisional interaction". There are three principal types of these interactions:[25]

1) Type one is the normal hydrogen bond variety. It is due to the formation of linear and near linear OH --- O bond system of different lengths formed during diffusional motion in the liquid.

2) A more common type of interaction occurs when the diffusional motion of water molecules does not follow OH --- O lines. This leads to nonlinear hydrogen bonds with variation of OH frequency.

3) The third type of interaction in solution is not of the hydrogen-bond type. One part of one or more water molecules moves close enough to an OH group to perturb the electron density; this interaction is called a "lateral collision".

All three of these interactions are expected to change the OH frequencies from their isolated value. Any particular molecule is expected to pass through all varieties of these interactions in the normal course of its motion through the liquid. The effect of these collisions

is to distort the water molecules in a variety of environments, altering both their potential energies and vibrational frequencies. This would tend to produce band broadening and give rise to a temperature effect. This picture provides a nearly continuous distribution of OH bonds experiencing various potential energy states.[21]

One approximation of the potential for each water molecule is a Maxwellian distribution[2] of distortion among water molecules with most molecules being in a somewhat distorted state while a minority are in a highly distorted one. This phenomenon also leads to a distribution of ν_{1d} and ν_{3d} states, these being vibrational eigenstates of the individual distorted OH bond vibrators in the liquid.

In addition, according to this model the breadth of the high frequency (less H-bonded) OH absorption band is perfectly consistent with a continuum theory of liquid water. However, it could also agree with the mixture model if enough discrete states are considered.

Vand and Senior[23] stated that a single continuum distribution of states leads to a satisfactory prediction of the thermodynamic properties of water, and that neglecting its continuum nature leads to unsatisfactory estimates of this data.[24] Vand and Senior[24] then also demonstrated that a three state continuum model and single continuum model,[25] both lead to reasonable predictions for the thermodynamic properties of water. (A paper by Senior et. al. indicates that he favors the three-state model.)[24,25]

Walrafen[26] proposed that there exist two types of water molecules in the liquid water: non-hydrogen-bonded and "lattice" water molecules.[7] He assigned separate V_3 and V_1 bands to each of these, and considered the superposition of these components as forming the OH stretching band of water. Walrafen examined the temperature variation of the Raman spectrum of water and found it could be made consistent with this two-state theory, thereby devaluing the continuum model.[26] However, even if only two states are assumed, there would probably be a fairly wide range of potential energy variation of these states due to the wide variety of H-bonded configurations possible. Because the three components of this H-bonded stretching overlap so much, it is impossible to assign an absorbance at a given frequency to a unique type of water molecule. However, it is possible to assign each band to a type of water (A, B, or C) molecule in a variety of environments.

CHAPTER IV

EXPERIMENTAL

The natural phenomenon of reflectance spectroscopy is exploited in our method of studying the themodynamics of liquid water.

Historical Background

Harrick[27] has pointed out perhaps the earliest recorded reference to the principle of internal reflectance spectroscopy - namely the observations of Isaac Newton more than 270 years ago. When light is reflected from an interface of two different optical media, say air and glass, the reflected rays show characteristics of the medium on the far surface of the glass.

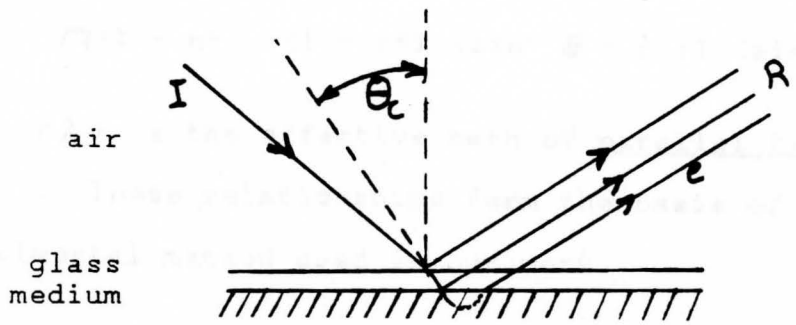

Therefore, it was obvious even then that some of the reflected light actually passes into this medium, but then returns to rejoin the reflected ray bundle. It is while this "evanescent wave" (e) is in the opposite medium that it can be affected (absorbed) at certain wavelengths characteristic of this medium, say water.

When the incident ray (I) approaches the interface at an angle greater than the critical angle (θ_c), it is "totally" reflected (not transmitted), yet these reflected rays also show characteristics of the lower medium. The depth of penetration of the wave (effective path length) can be calculated knowing the refractive indeces of the media, the geometry of the rays, and the wavelength of light.[27]

$$d_1/\lambda = n \cos \theta / \pi (1-n^2) (\sin^2\theta - n^2)^{1/2} \quad (1)$$

d_1/λ is the effective path length of perpendicular light in units of λ, the wavelength of light

θ is the angle of incidence

n is the refractive index ratio of the denser to the rarer medium

$$(d_{11}/\lambda) = n \cos \theta (2\sin^2 \theta - n^2)/ \quad (2)$$
$$\pi(1 - n^2) [(1 - n^2) (\sin^2 \theta - n^2)] (\sin^2 \theta - n^2)^{1/2}$$

(d_{11}/λ) is the effective path of <u>parallel light</u>, in units of λ. These relationships form the basis of the experimental method used in our work.

Experimental

All spectra were measured on a Digilab FTS-40, FTIR spectrometer internal reflectance circle cell, fitted with either ZnSe or Ge cylindrical crystals as internal reflectance elements. An annular space containing liquid H_2O or D_2O surrounds the central crystal, and this space was in turn surrounded by a heating jacket of circulated water, whose temperature was controlled by a thermostat.

The sample compartment of the ZnSe cell was dried by pumping dry N_2 through it. The cell was then placed in the optical compartment and water was circulated through the heating jacket, and a background was obtained at 25°C. This background spectrum was used for experiments at different temperatures; background spectra were also obtained at different temperatures, which shaved there was no temperature effect on the background spectrum. The sample compartment was filled with pure DI water or commercially available 99.9% D_2O, and a sample spectrum was obtained at temperatures from 25 to 90°C. Sample spectra were recorded in the absorbance mode (A), where $A=\log_{10}(1/T)$, and T is the transmittance spectrum. To produce a transmittance spectrum, the sample single-beam spectrum was divided by the background spectrum and displayed from 0 to 100%.

$$T\% = \frac{\text{Sample}}{\text{Background}} \times 100 \qquad (3)$$

The reason both ZnSe and Ge crystals were used was to show that the thermodynamic quantities being measured were independent of the cell material. FTIR results often show an intrinsic temperature dependence since refractive indeces (n in equation (1) and (2) depend on temperature in systematic ways. The fact that the present results are independent of crystal lends support to the interpretation, that the temperature effects are associated with the liquid samples.

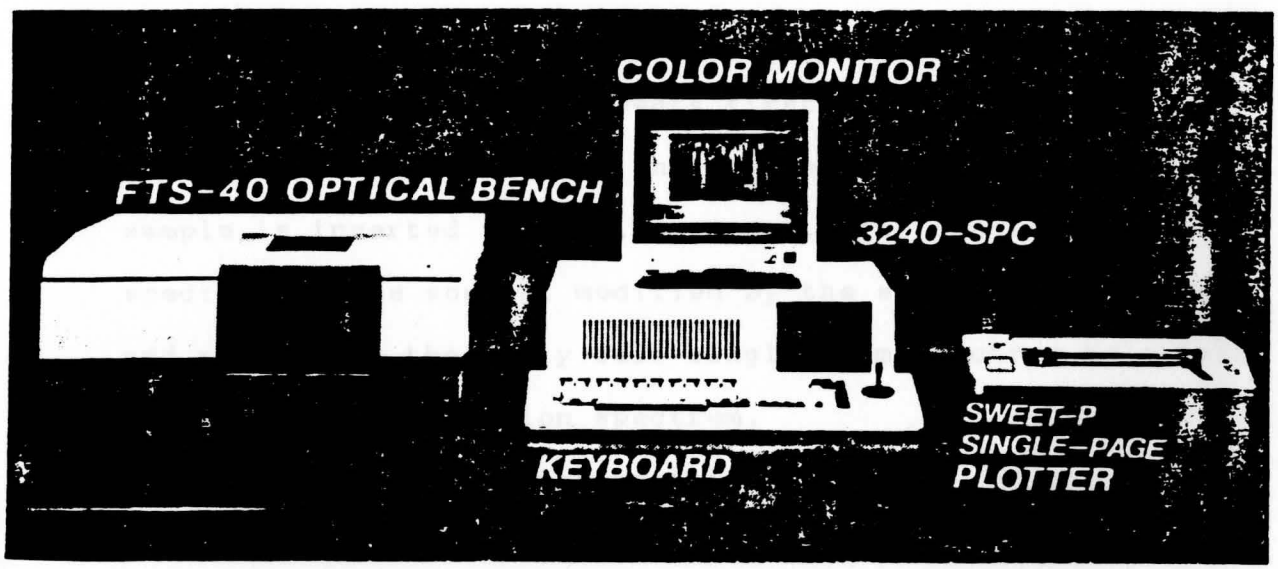

Fig. 3. The FTS-40 Spectrometer System

Instrument: The FTS-40 Spectrometer

The Bid Rad FTS-40 is a Fourier Transform Infrared spectrometer whose sensitivity is enhanced significantly by the computer application of the Fourier transform method. Infrared is the portion of the electromagnetic radiation between the visible and microwave regions, and here the mid infrared region of 4000 - 400cm^{-1} was used.

IR Theory: A molecule may absorb infrared radiation of an appropriate frequency to excite it from one vibrational or rotational state to another. When a beam of infrared energy is passed through a sample, the energy at certain frequencies is absorbed by the sample. A graph of energy absorbed versus frequency is the absorption spectrum of the sample. The spectrum is characteristic of the particular molecule and its molecular motions.

Digilab FTIR instruments first collect the spectrum of the source and store it in computer memory. Then the sample is inserted in the instrument. The single beam spectrum of the source, modified by the sample, is collected and ratioed to the empty cell single-beam spectrum to obtain the desired transmission spectrum.

The interferometer contains one fixed and one moveable mirror, and a beamsplitter. The beamsplitter transmits the radiation to the moving mirror and reflects the other half to the fixed mirror. The two beams are reflected back to the beamsplitter by these mirrors and recombined. The beams interfere constructively or

destructively depending on the position of the moving mirror and the frequency of the radiation. As the position of the moving mirror changes, the two beams will travel different distances before recombining. This optical path difference is called retardation.

The moving mirror is moved at constant velocity by a linear motor under computer control. The motion of the moving mirror continuously changes the retardation. As the moving mirror is displaced, the output beam intensity at each optical frequency changes. The frequency of this change depends upon the optical frequency and the speed of the moving mirror. Thus, the intensity of the light at each optical frequency varies at a particular rate, the output beam is therefore modulated by the interferometer. This modulated output beam is then directed through the sample compartment to the detector. The detector generates an electrical signal called an interferogram. The HeNe laser, operating at 632.8 nanometers, generates a reference signal which is used to measure the retardation and provide an internal clock. This clock enables the spectrometer electronics to sample the interferogram at precise intervals generating a digital signal compatible with the computer. The computer converts the interferogram into a single beam spectrum by a set of mathematical operations consisting of the Fourier transform.

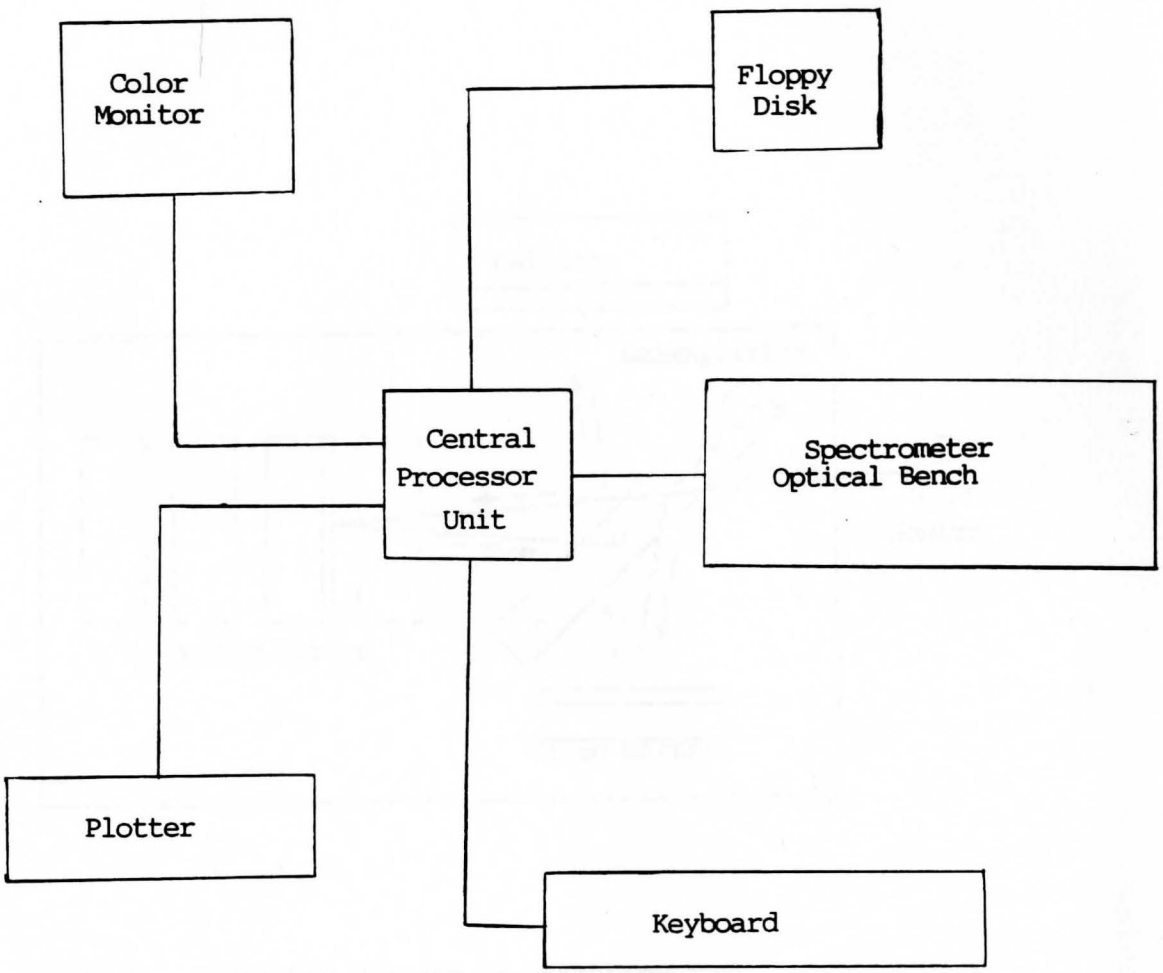

Fig. 4. Block diagram of the FTS-40 spectrometer system.

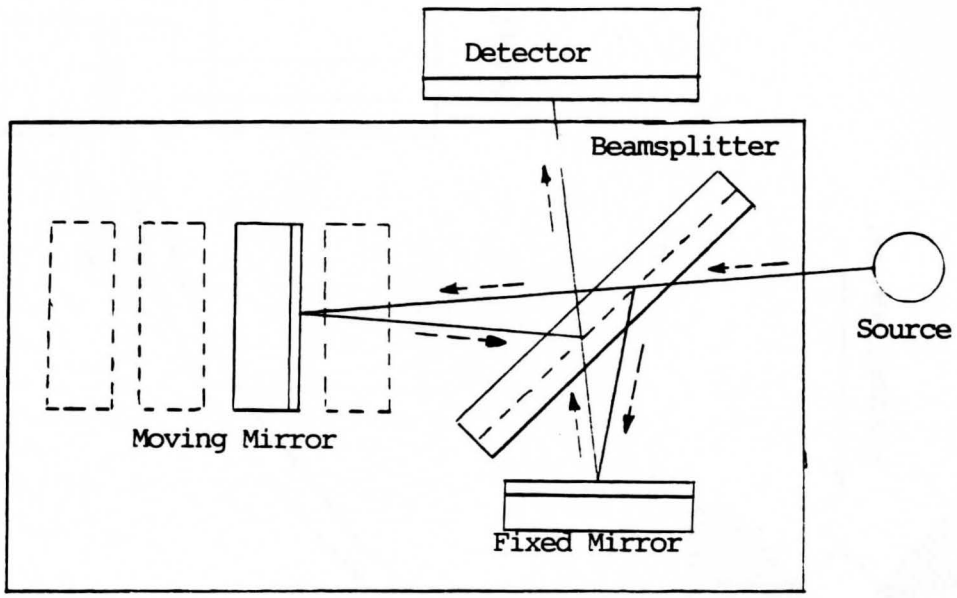

Fig. 5. Schematic diagram of interferometer

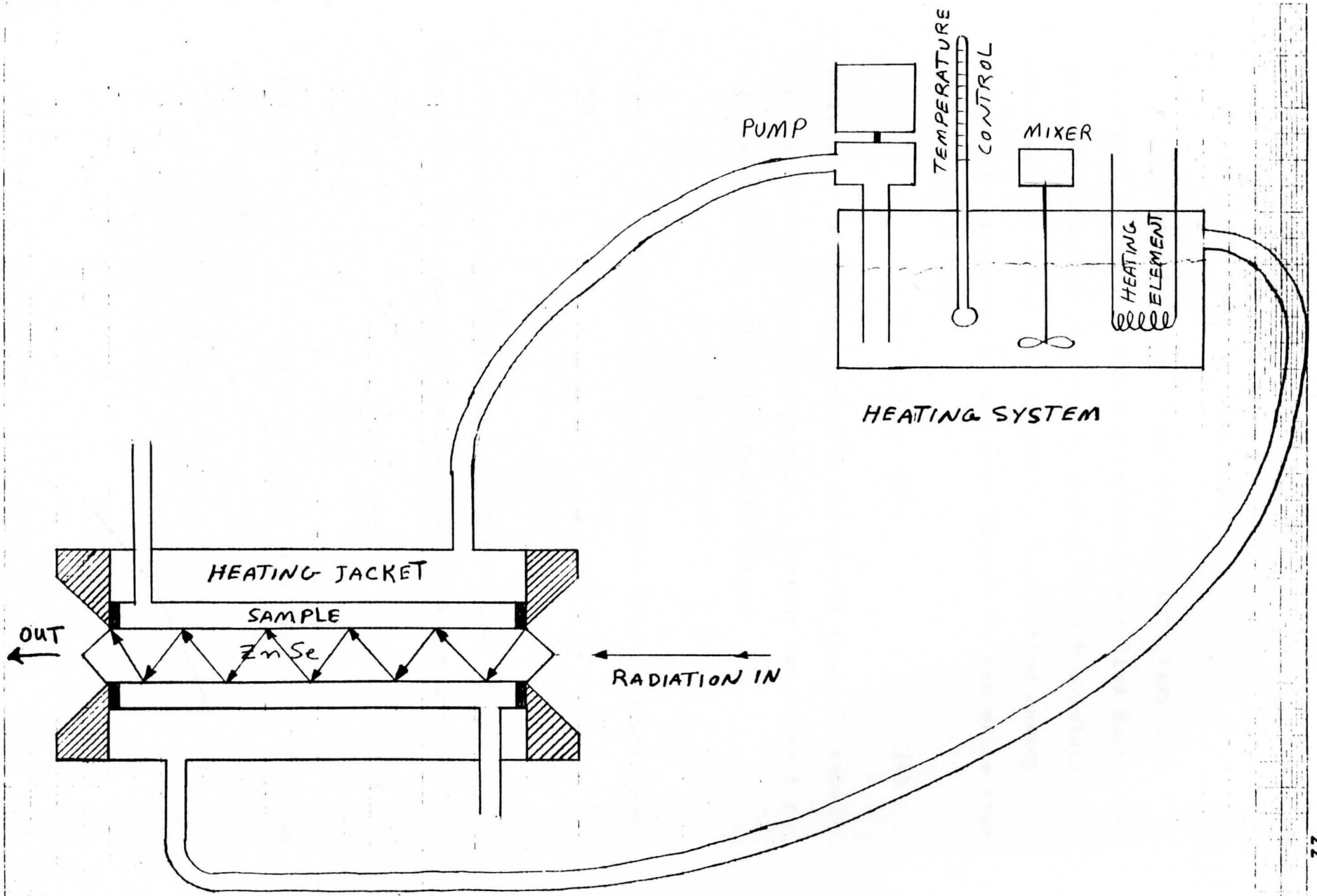

Fig. 6. Schematic diagram of the cell with heating jacket and heating system.

Beer's Law

The amount of radiation absorbed by a sample is described by the Beer-Bouguer-Lambert Law called Beer's Law. Consider radiation of power P_o passes through a solution at concentration C and path length l. Transmitted energy decreases exponentially with path length; We can write this in exponential form

$$T = \frac{P}{P_o} = 10^{-k_1 l} \qquad (4)$$

where k_1 is a constant and T is called the transmittance. Beer and Bernard each stated that a similar law holds for the transmittance (T) on the concentration

$$T = \frac{P}{P_o} = 10^{-k_2 c} \qquad (5)$$

where k_2 is a new constant, and putting this in logarithmic form

$$\log T = \log \frac{P}{P_o} = -k_2 c \qquad (6)$$

combining these two laws, we have Beer's Law, which describes T as dependent on both concentration and path length

$$T = \frac{P}{P_o} = -10^{-klc} \qquad (7)$$

where k here is a combined constant of k_1 and k_2. Then the absorbance A is

$$A = \log T = \log \frac{1}{T} = \log \frac{P_o}{P} = klc \qquad (8)$$

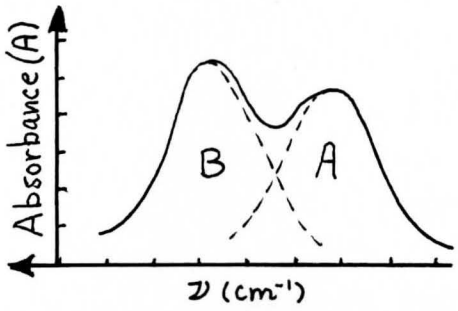

$$[C_A] = \frac{\int A_A \, d\nu}{k_A \, l}$$

$$B \rightleftharpoons A \qquad K_e = \frac{[C_A]}{[C_B]}$$

Figure 7. Schematic absorbance spectrum showing how equilibrium concentrations are obtained using Beer's Law.

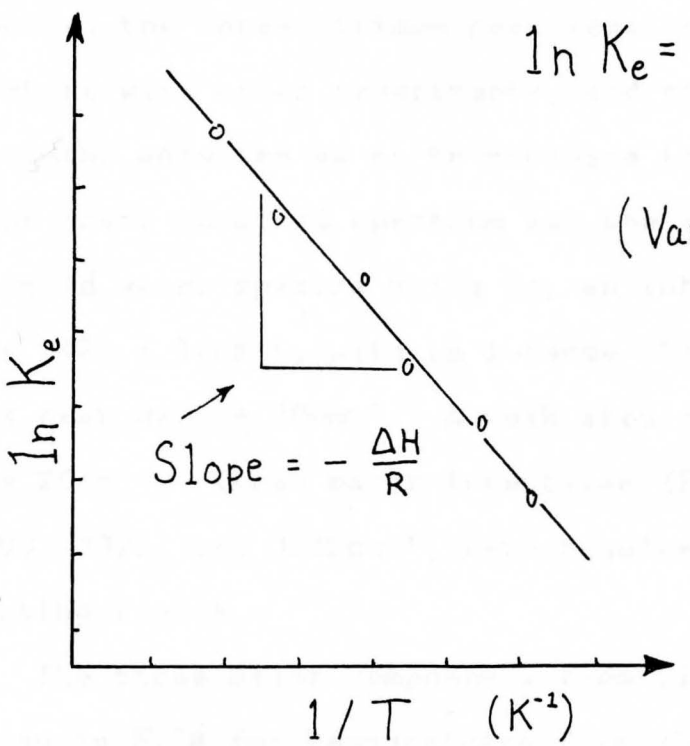

$$\ln K_e = -\frac{\Delta H}{RT} + \frac{\Delta S}{R}$$

(Van't Hoff)

Figure 8. Van't Hoff plot ($\ln K_e$ vs. 1/T) illustrating how thermodynamic data are obtained from experiment.

CHAPTER V

RESULTS AND DISCUSSIONS

General Discussion

H_2O Spectra with Ge Crystal

Each experimental spectrum showed the presence of at least three major overlapping components whose positions, intensities (absorbances), and widths could be generated smoothly be the Bandfit Program (Bio Rad accessory). In our procedure, the three optimum peak locations were chosen consistent with other experiments, and their intensities and half widths adjusted so as to minimize the difference between their combined spectrum and the experimental one. For liquid water spectra using Ge, an intensity maximum occurs 3425 $\pm$ 10cm^{-1}, with an intense (Fig. 9) shoulder occurs near 3225 $\pm$ 20cm^{-1}. A weak shoulder is evident near 3600 $\pm$ 20cm^{-1}. Three major Lorentzian (Fig. 10) components at 3200, 3375, and 3535cm^{-1}, were required to fit the OH stretching region.

The three major components from liquid H_2O were examined in FTIR for temperatures from 25 to 90°C. Intensities of two frequency components occuring above 3350 cm^{-1} were found to increase with temperature rise, whereas

intensity of the strong component having frequency below 3350 cm^{-1} was found to decrease. The pair of high frequency components above 3350 cm^{-1} were assigned to less H-bonded, and the low frequency part was assigned to more H-bonded, forms of water.

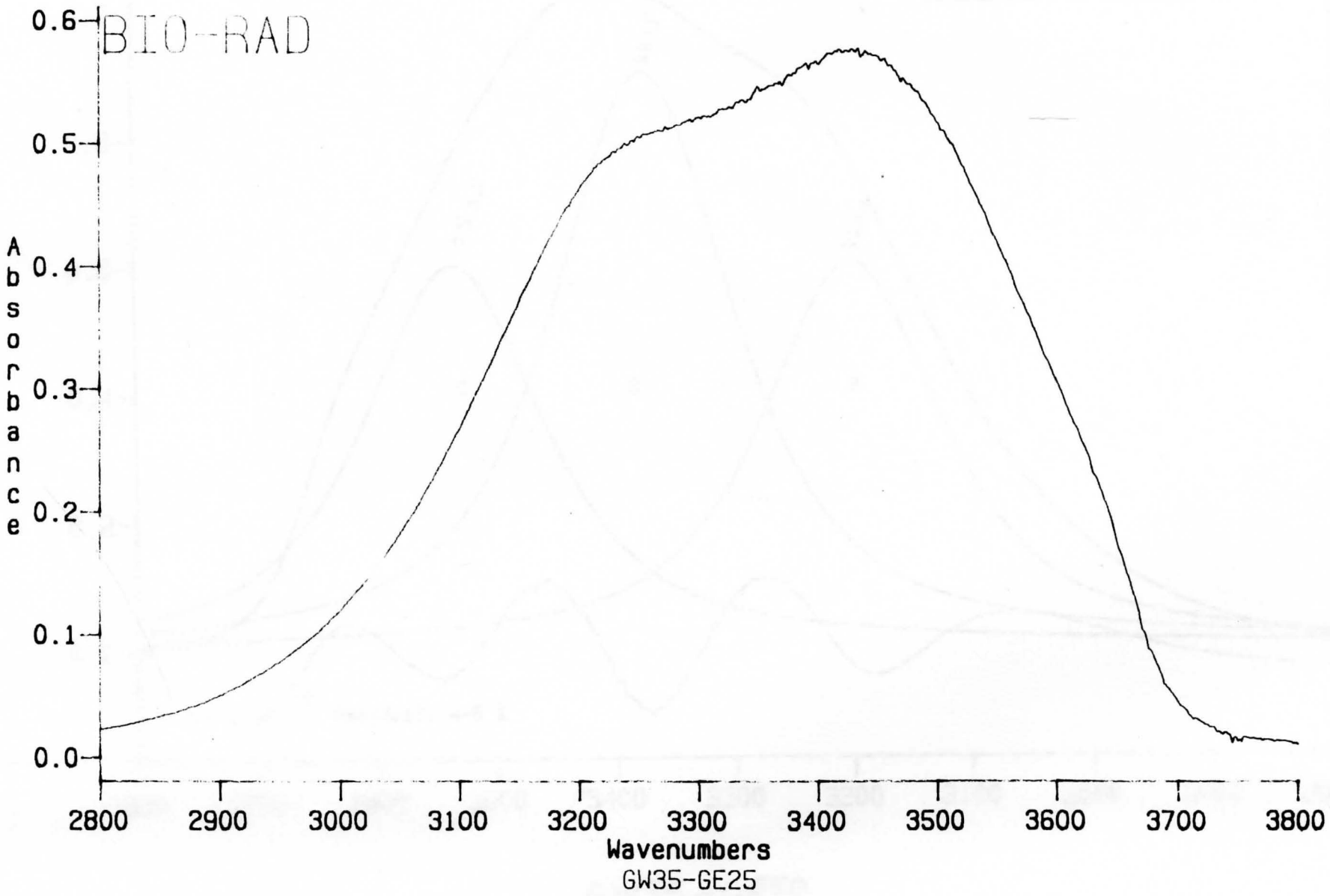

Fig. 9. FTIR internal reflectance spectrum of H_2o with Ge crystal at 35 C.

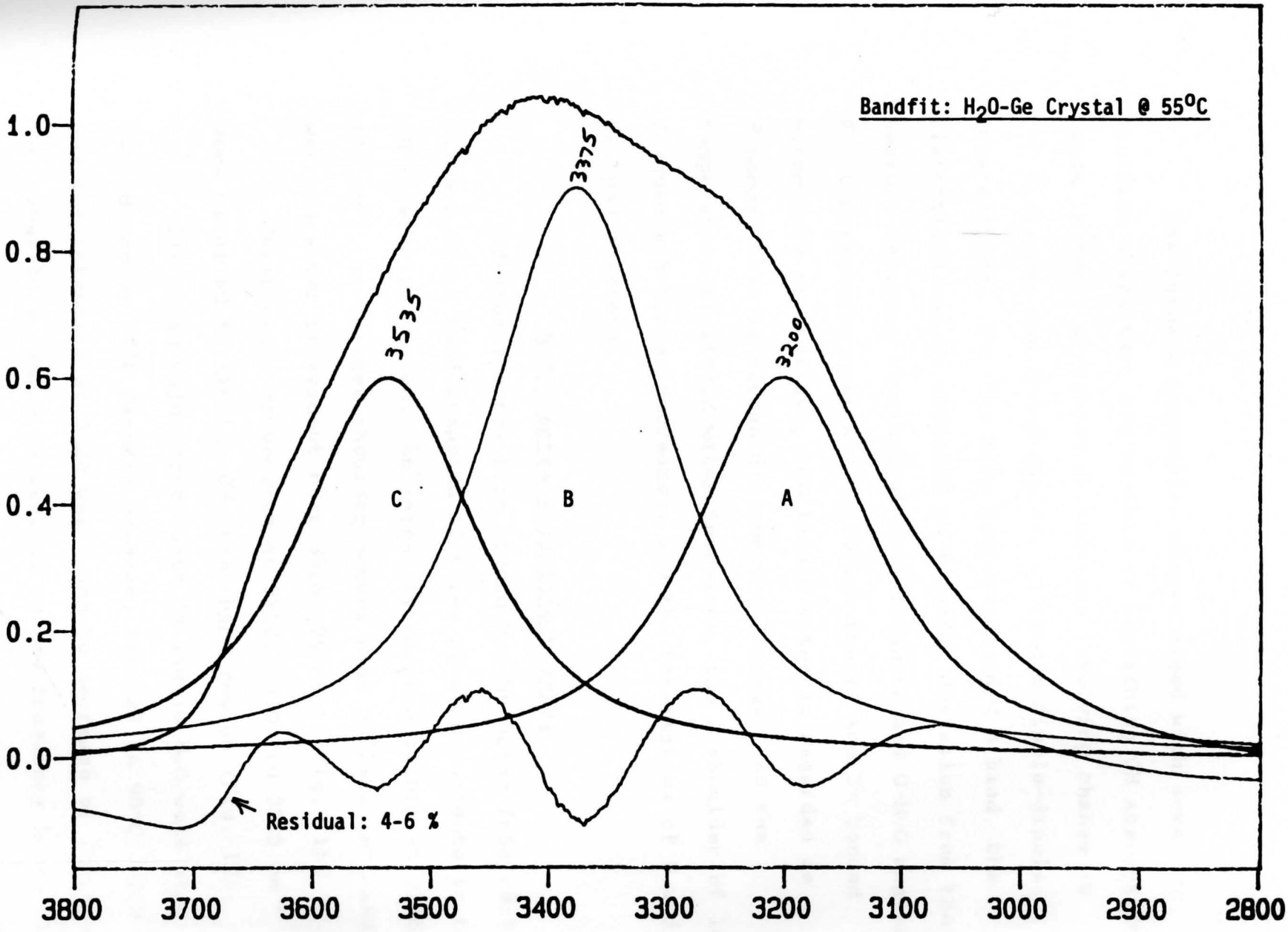

GW55-GE50

Fig. 10. Deconvoluted spectral components of experimental profile of water absorption with Ge crystal at 55°C.

The largely Lorentzian shapes mixed with some Gaussian character, are capable of explaining OH absorption bands in terms of random distortions involving change in O-O distances and O-H-O angles, or random dipole-dipole interactions. For the more hydrogen-bonded A band, the distortions may be regarded as a random deviation from the nearest-neighbor tetrahedral O-O distances and O-H-O angles. For temperatures near 25°C at which the 4- and 3- bonded structures predominate, the liquid water is regarded as a H-bonded that is tetrahedral on the average. As the temperature of liquid water increases, the A shoulder of low frequency H-bonded decreases, and the intensities of B and C regions increase.

H_2O Spectra with ZnSe Crystal

Infrared spectra from liquid H_2O by using ZnSe cell gives a broad band composed of three broad components in the OH stretching region. An intensity maximum occurs at 3225 $\pm$10 cm^{-1}, an intense shoulder occurs near 3370$\pm$25 cm^{-1} and a weak shoulder is evident near 3525 $\pm$25 cm-1 (Fig. 11).

Three major components at 3220, 3350 and 3525 cm^{-1} were required to fit the OH stretching region (Fig. 12).

The three major components in liquid H_2O were also reproduced by FTIR Bandfit program, from 25 to 90°C. The maximum intensity at 3220 was found to decrease by increase in temperature, which correspond to low frequency A and it is H-bonded region. But intensities of shoulder at 3370 and 3525 cm^{-1} increases by rise in temperature that correspond

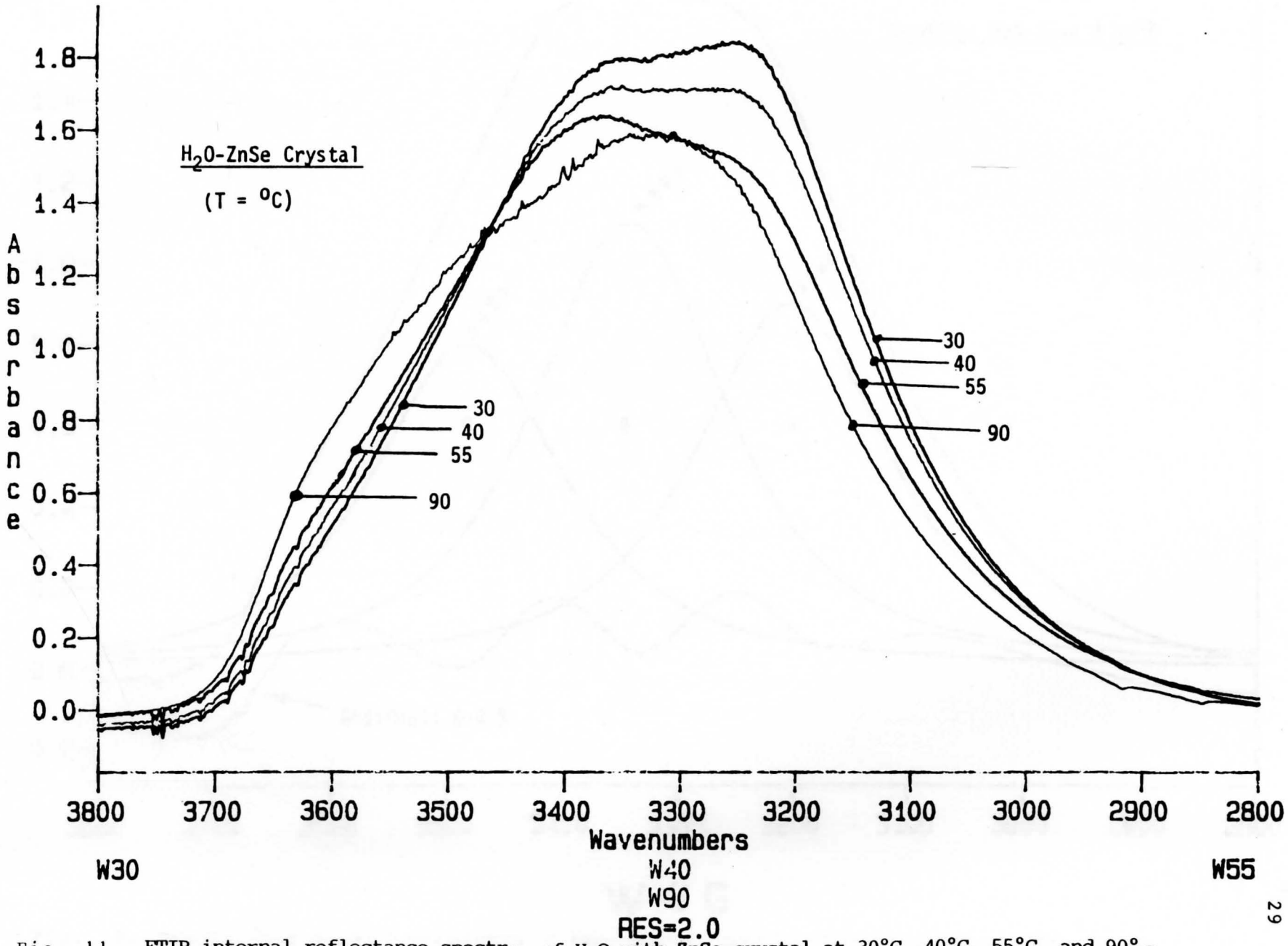

Fig. 11. FTIR internal reflectance spectra of H_2O with ZnSe crystal at 30°C, 40°C, 55°C, and 90°C.

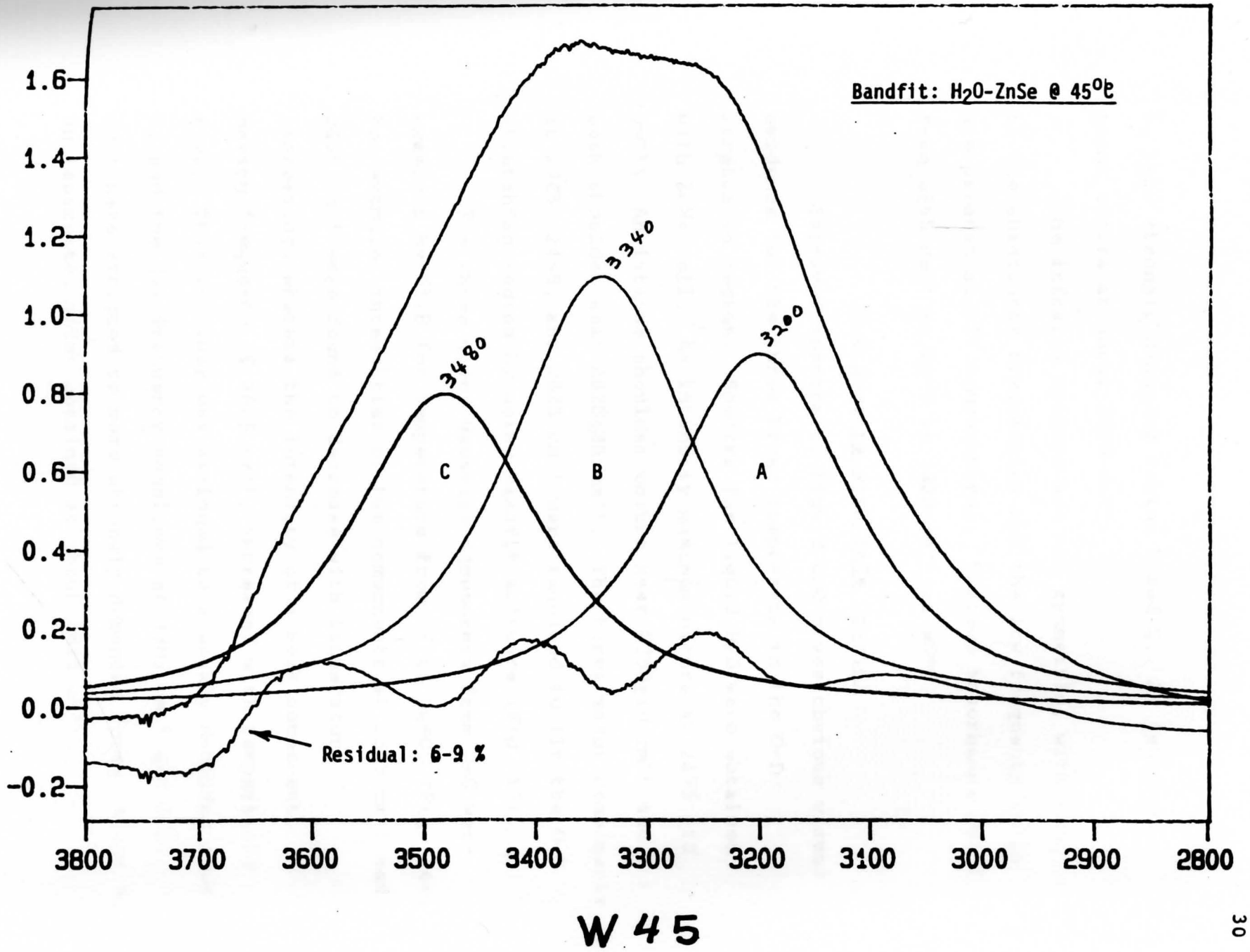

Fig. 12. Deconvoluted spectral components of experimental profile of H_2O absorption with ZnSe crystal at 45°C.

to less strongly H-bonded region B and C. An isosbestic point occurs at about 3500 cm^{-1}.

The infrared spectra are not symmetric, with respect to the absorbance frequencies and the low frequency tails are present at all temperatures. Maximum absorbance shift from 3245 cm^{-1} at 26°C to 3320 cm^{-1} at 90°C.

D_2O Spectra with ZnSe Crystal

Infrared spectra of liquid D_2O gives obvious visual evidence for the three broad components in the O-D stretching region. Spectra for liquid D_2O were obtained with ZnSe cell. An intensity maximum occurs at 2475 $\pm$10 cm^{-1}. An intense shoulder occurs near 2380$\pm$10 cm^{-1} and a weak shoulder near 2625$\pm$25 cm^{-1}. The three major components at 2385, 2495, and 2625 cm^{-1} were required to fit the O-D stretching region by using Bandfit software (Fig. 13).

The three major Gaussian components from D_2O were examined by FTIR for temperature from 25 to 90°C, (Fig. 14). For example, intensities of two components at 2385 cm^{-1} and 2495 cm^{-1} were found to decrease with temperature increasing, whereas the intensity of a weak component, having frequency of 2625 cm^{-1}, increased with temperature rise. This shoulder was assigned to a weakly H-bonded from C, and the low frequency shoulders at 2385 cm^{-1} and 2495 cm^{-1} were assigned to more strongly H-bonded forms, A and B. An isosbestic point obtained at about 2625 cm^{-1}.

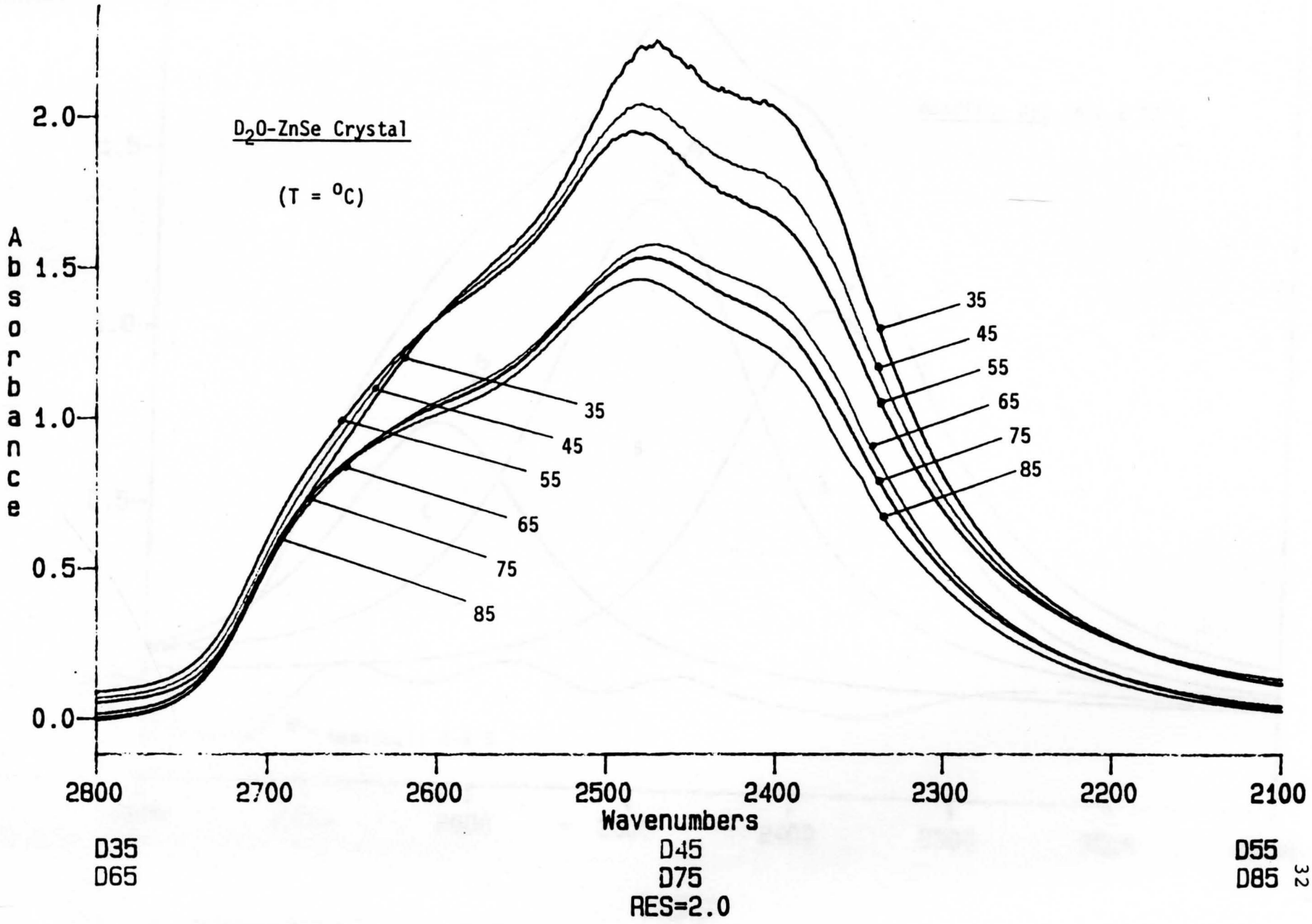

Fig. 13. FTIR internal reflectance spectra of D_2O with ZnSe crystal at 35°C, 45°C, 55°C, 65°C, 75°C, and 85°C.

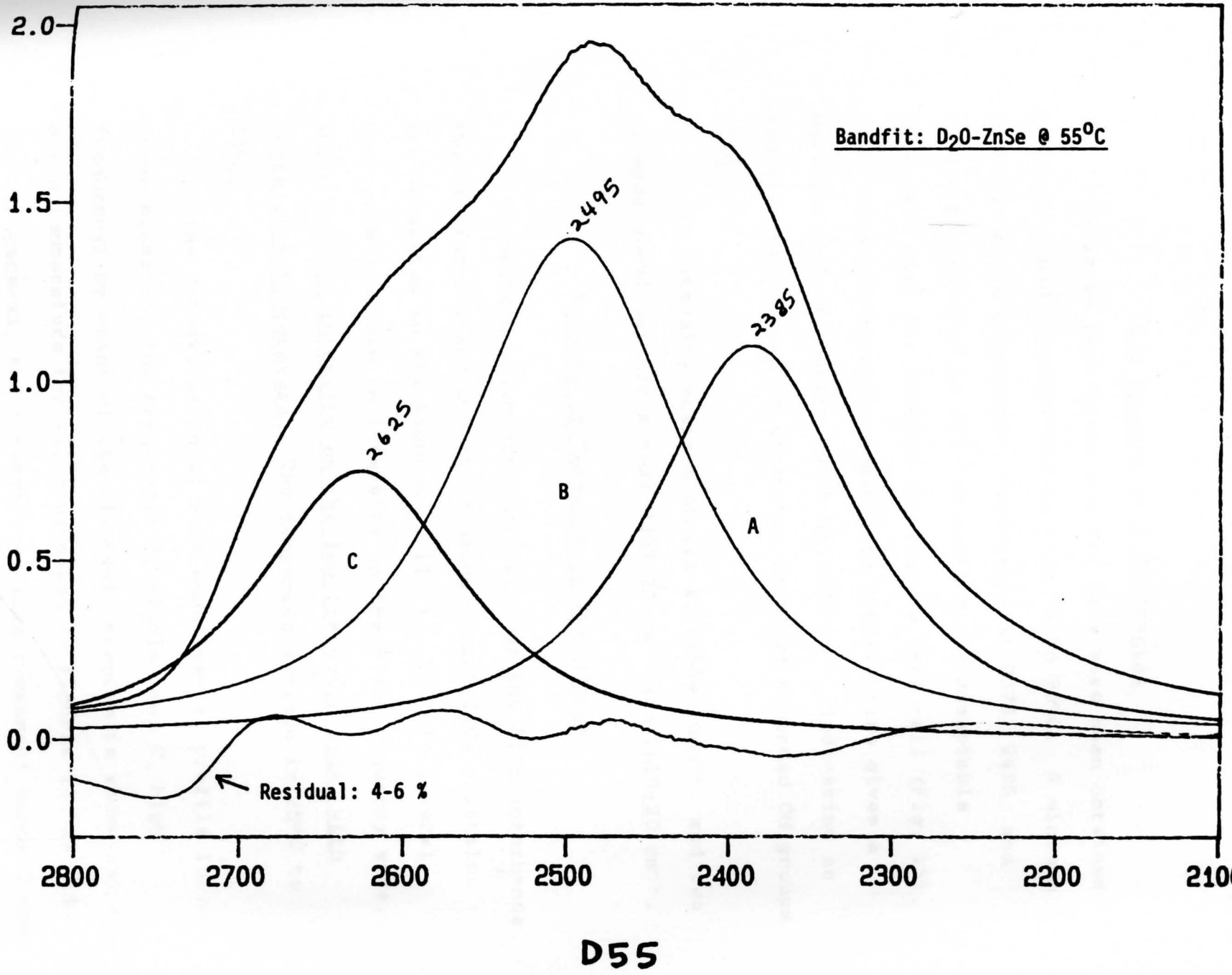

Fig. 14. Deconvoluted spectral components of experimental profile of D_2O absorption with ZnSe crystal at 55°C.

D_2O Spectra with Ge Crystal

Infrared absorbance spectra have also been obtained for D_2O liquid at temperatures from 25 to 90°C. A minimum of three broad components, centered near 2375, 2495, and 2630 were required to fit the contour, in acceptable agreement with the spectra obtained by ZnSe cell (Fig. 15).

The quantitative absorbance spectra also gives a well defined isosbestic point at 2380 cm^{-1}, indicating an equilibrium between at least two forms of H-bonded OH groups (Fig. 16).

An intensity maximum occurs at 2495$\pm$ 10cm^{-1}, and two intense shoulders occur near 2385$\pm$20 cm^{-1} and 2610$\pm$20 cm^{-1}.

Results of Temperature Dependence

Temperature dependent profiles of the FTIR absorbance spectra for H_2O and D_2O, both using Ge and ZnSe crystals, are presented in the Figures 9, 11, 13, 16. In general, they show a growth in intensity on the high frequency side, and a loss of intensity on the low frequency side, with increasing temperature. The temperature range is 25°C to 90°C.

The deconvolution of each experimental profile into three bands (A, low frequency; B, middle, and C, high frequency) by means of the "Bandfit" program is shown for a given temperature for all four cases in Figures 10, 12, 14, 15. In general, the intensity of such component bands B and C grow at the expense of A, with increasing temperature. Once the band parameters were developed, as far as position,

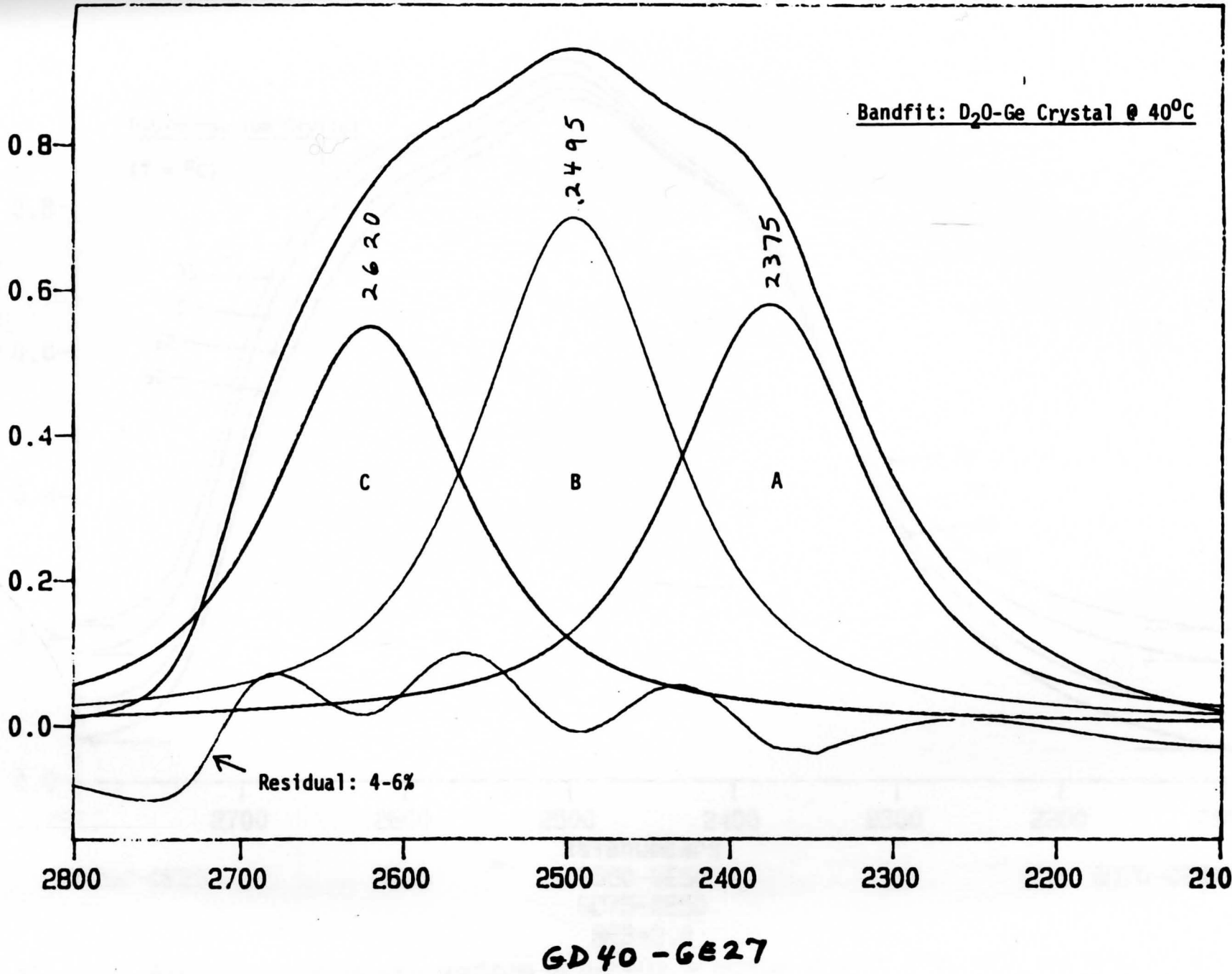

Fig. 15. Deconvoluted spectral components of experimental profile of D_2O absorption with Ge crystal at 40°C.

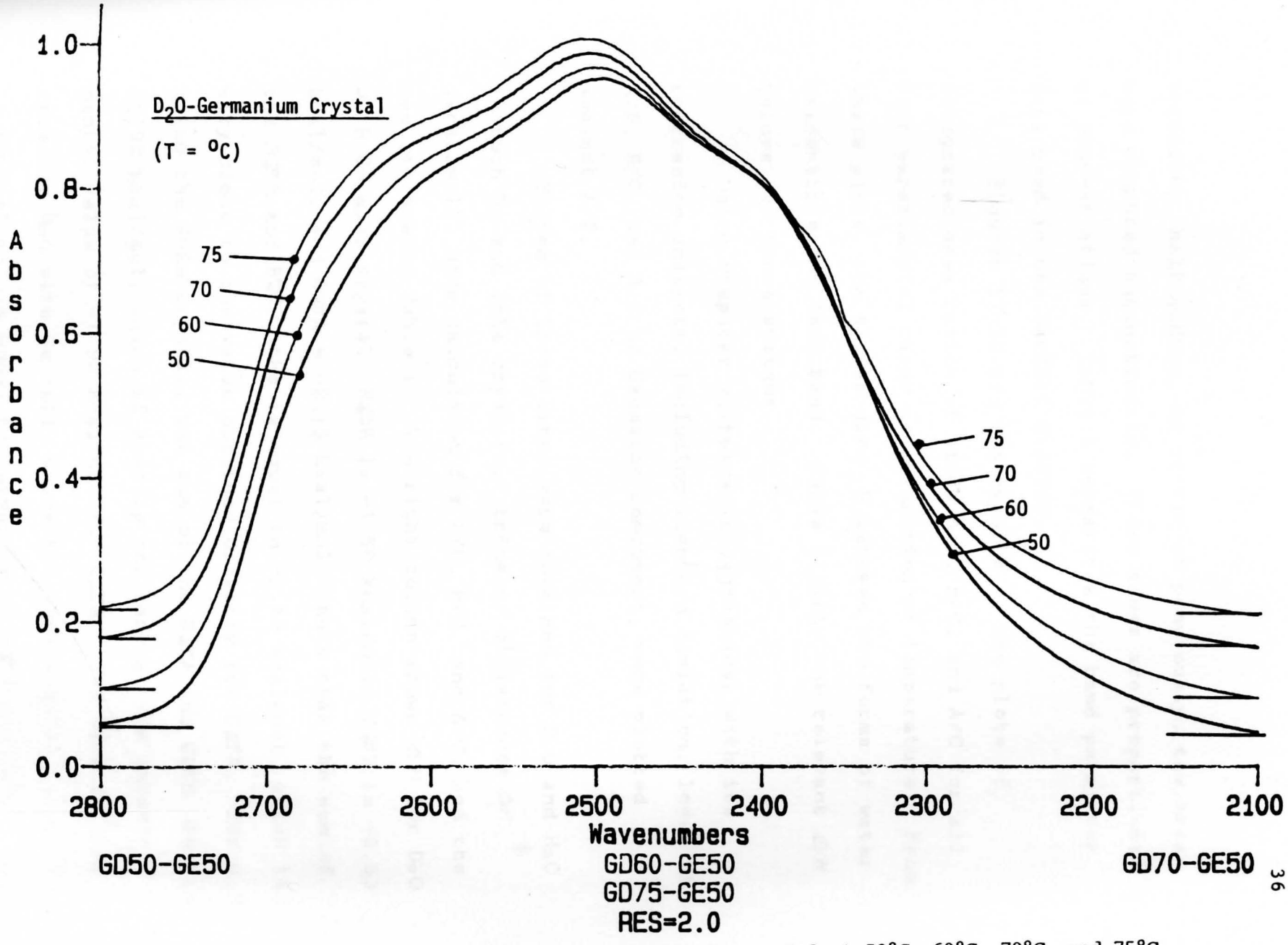

Fig. 16. FTIR internal reflectance spectrums of D_2O with Ge crystal at 50°C, 60°C, 70°C, and 75°C.

intensity, half widths, as mentioned previously, the areas were computed automatically. These areas are proportional to concentrations. Table 2 summarizes the band parameter data used in the Bandfit program.

Figures 17-20 are the results of the plots of integrated area ratios of bands A/B, B/C, and A/C for all four experimental cases as a function of temperature. From these plots, the slopes give H between the forms of water responsible for each band. Table 1 lists the relevant ΔH values for these systems.

Using computer software (Energraphics) with its regression analysis, including standard deviation, $\log_{10}$ of A/B, B/C, and A/C of Gaussian component, were plotted against **1/T.**

Slopes of these lines were obtained for D_2O and H_2O in both Ge and ZnSe crystals. Enthalpy differences ΔH (kcal/mol), were calculated for A/B, B/C, and A/C, and the results are in Table 1. The right column shows ΔH for D_2O with Ge kcal crystal, B$\rightleftarrows$A is -1.50 kcal/mol, C$\rightleftarrows$B is -0.63 kcal/mol, and C$\rightleftarrows$A = -2.15 kcal/mol. Note that the sum of the B$\rightleftarrows$A and B$\rightleftarrows$C ΔHs is equal to -2.13 kcal/mol, which is very close to the value obtained directly for C$\rightleftarrows$A. For D_2O using the ZnSe crystal, the sum of the B$\rightleftarrows$A and C$\rightleftarrows$B ΔHs is -1.98 kcal/mol, which is exactly the same as the experimental value of -1.98 kcal/mol for C$\rightleftarrows$A. The same is also true for H_2O with Ge cell, where the experimental value of -1.60 kcal/mol is equal to summation of B$\rightleftarrows$A and C$\rightleftarrows$B (-1.60 kcal/mol).

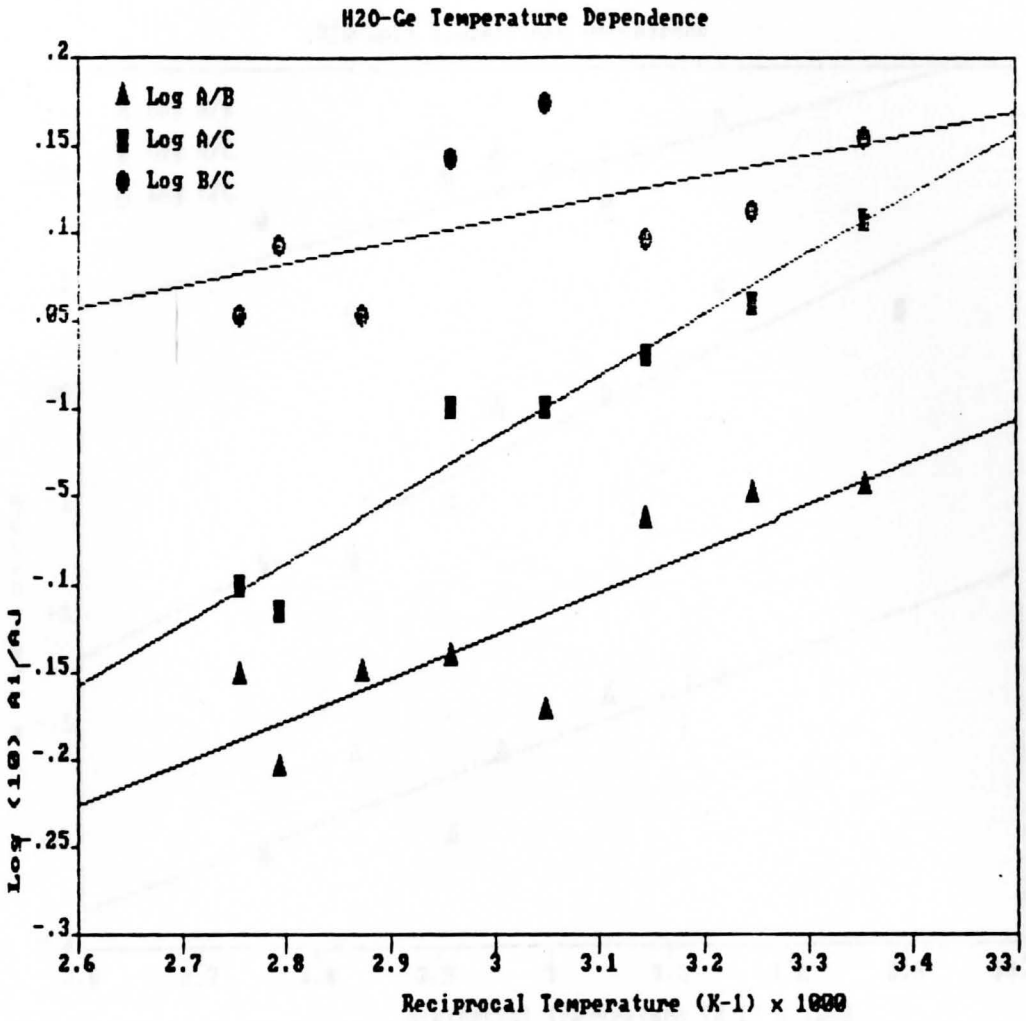

THE REGRESSION POLYNOMIAL OF LINE 1 -

(-8.579E-01) + (2.429E-01)*X
THE VARIANCE - 7.883E-04

THE REGRESSION POLYNOMIAL OF LINE 2 -

(-1.066E+00) + (3.495E-01)*X
THE VARIANCE - 2.489E-04

THE REGRESSION POLYNOMIAL OF LINE 3 -

(-2.665E-01) + (1.243E-01)*X
THE VARIANCE - 1.113E-03

Fig. 17. Plot of integrated area of bands A/B, B/C, and A/C for experimental cases of H_2O with Ge crystal vs reciprocal temperature.

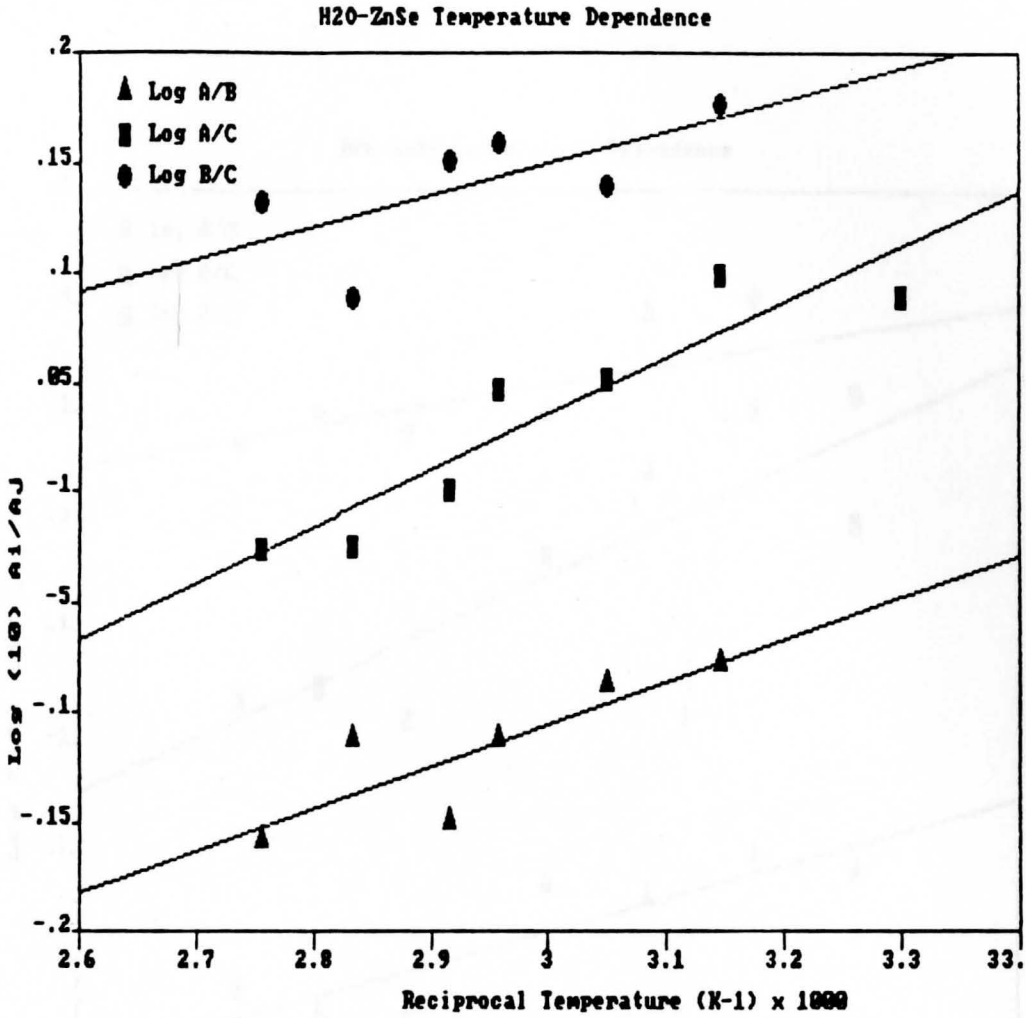

THE REGRESSION POLYNOMIAL OF LINE 1 -

(-6.799E-01) + (1.912E-01)*X
THE VARIANCE - 2.603E-04

THE REGRESSION POLYNOMIAL OF LINE 2 -

(-7.252E-01) + (2.533E-01)*X
THE VARIANCE - 3.136E-04

THE REGRESSION POLYNOMIAL OF LINE 3 -

(-2.857E-01) + (1.450E-01)*X
THE VARIANCE - 4.168E-04

Fig. 18. Plot of integrated area of bands A/B, B/C, and A/C for experimental cases of H_2O with ZnSe crystal vs reciprocal temperature.

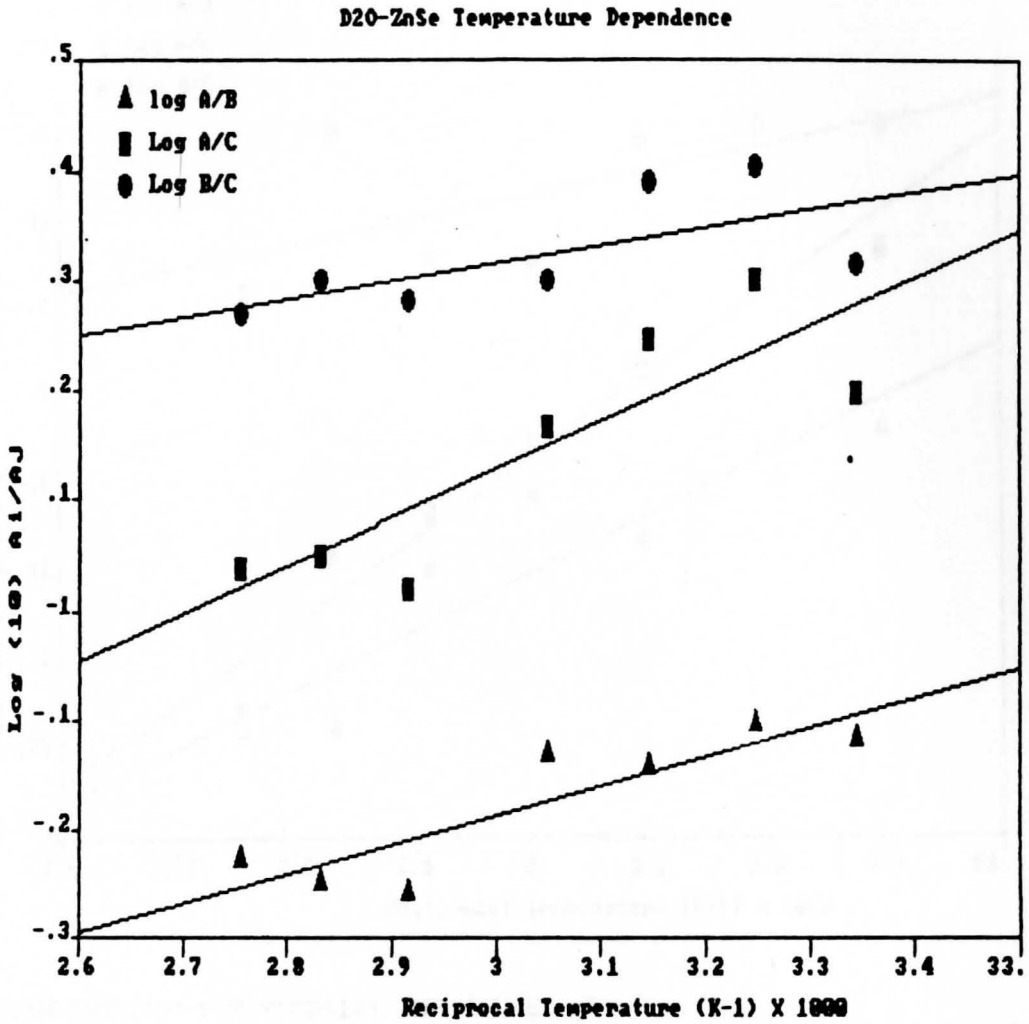

THE REGRESSION POLYNOMIAL OF LINE 1 -

(-9.984E-01) + (2.700E-01)*X
THE VARIANCE - 8.319E-04

THE REGRESSION POLYNOMIAL OF LINE 2 -

(-1.169E+00) + (4.321E-01)*X
THE VARIANCE - 2.750E-03

THE REGRESSION POLYNOMIAL OF LINE 3 -

(-1.702E-01) + (1.620E-01)*X
THE VARIANCE - 1.336E-03

Fig. 19. Plot of integrated area of bands A/B, B/C, and A/C for experimental cases of D_2O with ZnSe crystal vs reciprocal temperature.

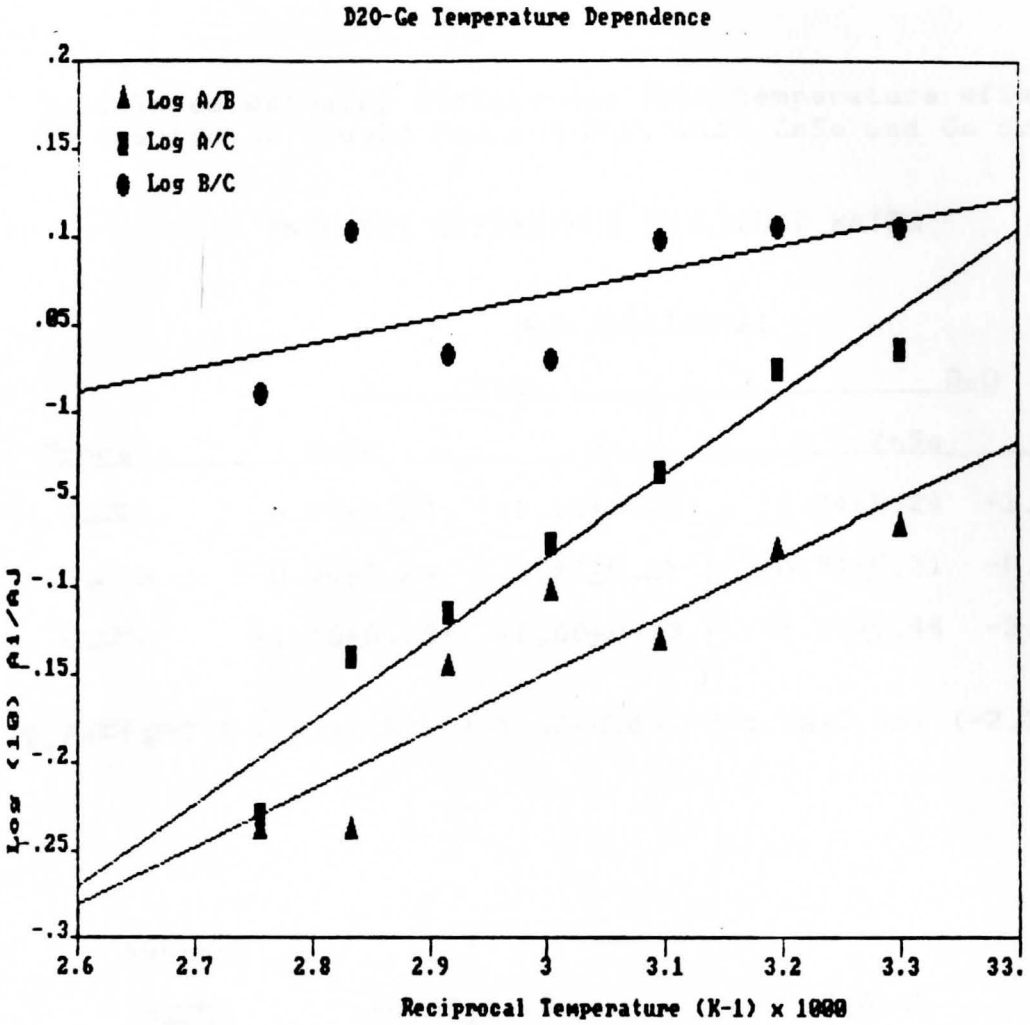

THE REGRESSION POLYNOMIAL OF LINE 1 -

(-1.138E+00) + (3.295E-01)*X
THE VARIANCE - 6.877E-04

THE REGRESSION POLYNOMIAL OF LINE 2 -

(-1.493E+00) + (4.698E-01)*X
THE VARIANCE - 3.251E-04

THE REGRESSION POLYNOMIAL OF LINE 3 -

(-3.473E-01) + (1.379E-01)*X
THE VARIANCE - 9.202E-04

Fig. 20. Plot of integrated area of bands A/B. B/C. and A/C for experimental cases of D_2O with Ge crystal vs reciprocal temperature.

TABLE 1

Calculated enthalpy differences from temperature effects on IR spectra of liquid H_2O and D_2O, with ZnSe and Ge crystals.

ENTHALPY DIFFERENCE IN LIQUID WATER

ΔH (kcal/mol)

	H_2O		D_2O	
Process	ZnSe	Ge	ZnSe	Ge
B⇄A	-0.87±0.23	-1.11±0.22	-1.24±0.24	-1.50±0.25
C⇄B	-0.66±0.29	-0.57±0.27	-0.74±0.31	-0.63±0.28
C⇄A	-1.16±0.18*	-1.60±0.13	-1.98±0.44	-2.15±0.17
≶ A⇄B⇄C	(-1.53±0.52)	(-1.60±0.49)	(-1.98±0.55)	(-2.13±0.53)

Average		
B⇄A	-0.98±0.22	-1.37±0.25
C⇄B	-0.62±0.28	-0.68±0.30
C⇄A	-1.57±0.16	-2.07±0.30

* RMS 5-10%; typical RMS 3-5%

$\sqrt{\frac{M_D}{M_H}} = 1.414 \qquad \frac{1.37}{.98} = 1.40 \qquad \frac{2.07}{1.57} = 1.32$

For H_2O with ZnSe, summation of A⇌B, B⇌C is equal to -1.53 kcal/mol, which is somewhat different than the experimental ΔH value of -1.16 kcal/mol for A⇌C though it is within the combined experimental errors of both. This discrepancy can be explained by the RMS error from the Bandfit program, which was about 9-10% in this case only. (The RMS was 3-5% for other cases of experiments.)

It is noteworthy also that the ratio of the three ΔH values for D_2O/H_2O (namely A/B and A/C) are close to 1.4, the square root of the mass ratio, D/H, indicating a primary isotope effect in the potential energy wells (Fig. 21).

The fact that in all four cases with D_2O and H_2O, independent of crystal, the entholpy differences between species A⇌B and B⇌C combined to give the result also found independently for A⇌C strongly supports the equilibrium model proposed.

CHAPTER VI

Conclusion

Water molecules exist in liquid water in one of three states, A, B, and C, each with a separate band of absorption frequency which overlap. We consider the superposition of these three components to form the complex OH stretching absorbance bands of water.

A three-state equilibrium distribution of water molecules in the liquid leads to a self-consistent prediction of the enthalpic thermodynamic properties of these types of water.

This interpretation is consistent with a "breathing cavity" model, that is composed of a centinuum distribution of three equilibrium species of water molecules A, B, and C, as yet unspecified in detail. A is the most stable one of the three configurations and C is the least stable one, in liquid D_2O or water. (Fig. 22)

There are barriers on the potential energy surface leading from one configuration to another which provide for the stablization of these types of water molecules.

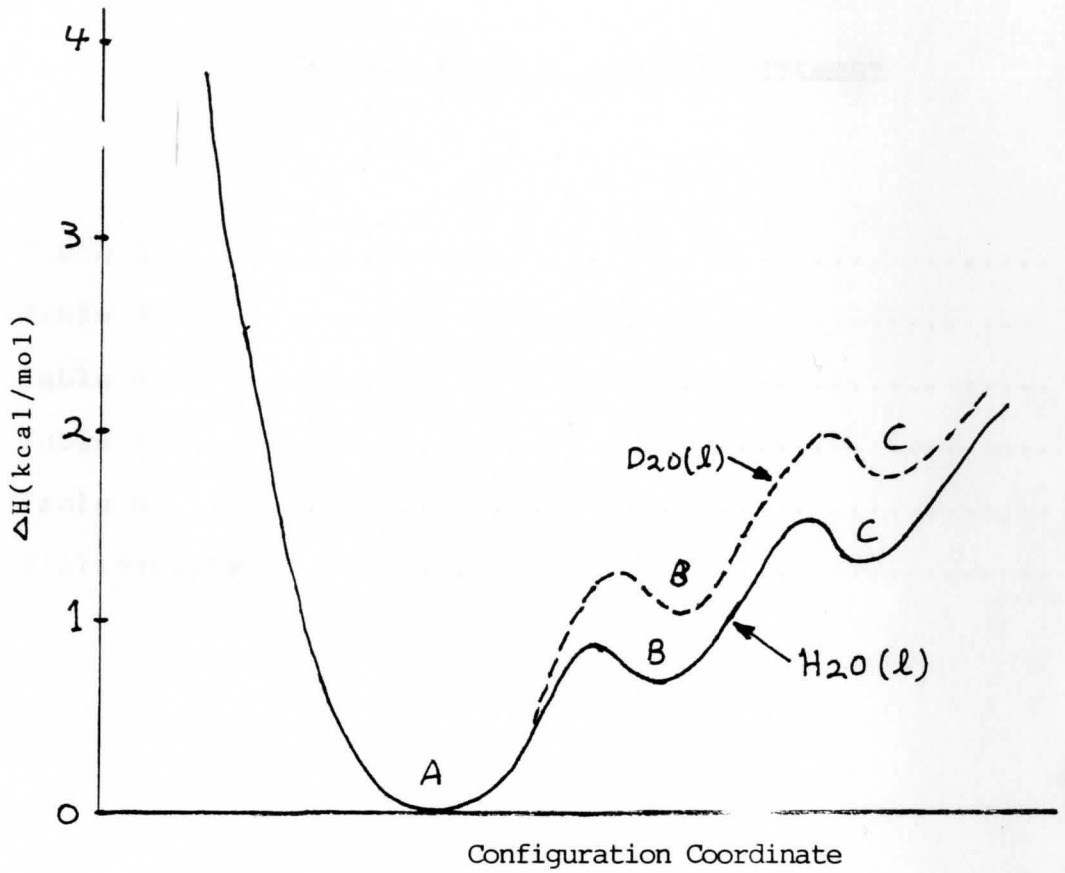

Fig. 21. Energy Diagram of Water Configuration

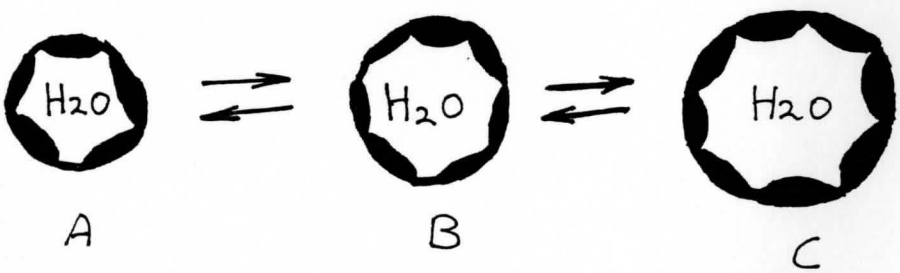

Fig. 22. Breathing Cavity Model

APPENDIX

Tables, Figures and Bibliography

TABLE 2

BAND PARAMETERS OF OH STRETCHING
ABSORPTION BANDS OF LIQUID H_2O AND D_2O

Sample	Crystal		Bands A	B	C
H_2O	D_2O	Band Center	3200-3220	3340-3350	3480-3525
		Half Width	100	100	100
Range -		% Gaussian	25	25	25
Change With T		I	0.8-1.1	1.1-1.3	0.8-0.9
		Area	190-262	262-303	190-214
H_2O	Ge	Band Center	3200	3375	3525
		Half Width	90-100	90-100	90-100
Range -		% Gaussian	25-50	25-50	25-50
Change With T		I	0.4-0.65	0.45-0.9	.35-.75
		Area	85-158	96-224	75-198
D_2O	ZnSe	Band Center	2385-2390	2485-2500	2610-2635
		Half Width	70-75	70-80	70-75
Range -		% Gaussian	20-25	20-25	20-25
Change With T		I	0.7-1.3	1.1-1.5	0.67-0.7
		Area	114-227	192-289	103-131
D_2O	ZnSe	Band Center	2385	2495	2620-2630
		Half Width	70-85	70-85	70-85
Range -		% Gaussian	20-25	20-25	20-25
Change With T		I	0.4-0.6	0.7-0.75	0.55-0.65
		Area	65-100	114-139	89-129

TABLE 3

INTEGRATED AREA OF BANDS A/B, B/C, AND A/C FOR EXPERIMENTAL CASES OF H_2O WITH ZnSe CRYSTAL.

	log A/B	log A/C	log B/C	1/T
W30	.098	.088	-.010	3.300×10^{-3}
W45	-.079	.098	.177	3.145×10^{-3}
W55	-.088	.051	.139	3.049×10^{-3}
W65	-.113	.046	.159	2.958×10^{-3}
W70	-.151	0	.151	2.915×10^{-3}
W80	-.113	-.025	.088	2.833×10^{-3}
W90	-1.59	-.026	.132	2.755×10^{-3}

TABLE 4

INTEGRATED AREA OF BANDS A/B, B/C, AND A/C FOR EXPERIMENTAL CASES OF H_2O WITH Ge CRYSTAL.

	log A/B	log A/C	log B/C	1/T
GW25-GE25	-.047	.107	.154	3.355×10^{-3}
GW35-GE25	-.052	.059	.112	3.246×10^{-3}
GW45-GE25	-.065	.029	.095	3.145×10^{-3}
GW55-GE50	-.173	0	.173	3.048×10^{-3}
GW65-GE50	-.142	0	.142	2.958×10^{-3}
GW75-GE50	-.152	.098	.053	2.873×10^{-3}
GW85-GE85	-.206	-.114	+.092	2.793×10^{-3}
GW90-GE85	-.153	-.10	.053	2.755×10^{-3}

TABLE 5

INTEGRATED AREA OF BANDS A/B, B/C, AND A/C FOR EXPERIMENTAL CASES OF D_2O WITH ZnSe CRYSTAL.

	log A/B	log A/C	log B/C	1/T
D 26	-.118	.197	.315	3.344×10^{-3}
D 35	-.105	.299	.404	3.247×10^{-3}
D 45	-.144	.246	.39	3.145×10^{-3}
D 55	-.133	.166	.299	3.048×10^{-3}
D 70	-.26	.02	.28	2.915×10^{-3}
D 80	-.25	.05	.30	2.832×10^{-3}
D 90	-.23	.04	.27	2.755×10^{-3}

TABLE 6

INTEGRATED AREA OF BANDS A/B, B/C, AND A/C FOR EXPERIMENTAL CASES OF D_2O WITH Ge CRYSTAL.

	log A/B	log A/C	log B/C	1/T
GD30-GE27	-.068	.036	.104	10.89×10^{-4}
GD40-GE27	-.081	.023	.104	10.208×10^{-4}
GD50-GE50	-.133	.036	.097	9.585×10^{-4}
GD60-GE50	-.104	.075	.029	9.018×10^{-4}
GD70-GE50	-.147	.115	.032	8.497×10^{-4}
GD80-GE85	-.24	.14	.103	8.025×10^{-4}
GD90-GE85	-.24	.23	.01	7.590×10^{-4}

BIBLIOGRAPHY

1. J. D. Bernal and R. H. Fowler, J. Chem. Phys. 1, 515 (1933).

2. L. Pauling "The Nature of the Chemical Bond", 3rd ed., Cornell University Press, Ithaca, New York (1960).

3. G. E. Walrafen, J. Chem. Phys. 40, 3249 (1964).

4. J. Del Bene and J. A. Pople Chem. Phys. 52, 4858 (1970).

5. J. Del Bene and J. A. Pople Chem. Phys. Letters 4, 426 (1969).

6. J. W. Schultz and D. F. Hornig, J. Phys. Chem. 65, 2131 (1961).

7. W. R. Busing and D. F. Hornig, J. Phys. Chem. 65, 284 (1961).

8. T. T. Wall and D. F. Hornig, J. Chem. Phys. 43, 2079 (1965).

9. H. S. Frank and W. Y. Wen, Discussions Faraday Soc. 24, 133 (1957).

10. H. S. Frank, Proc. Roy. Soc. (London) A247, 481 (1958).

11. H. S. Frank, Proc. Roy. Soc. (London) A247, 481 (1958).

12. H. S. Frank and W. Y. Wen, Disc. Faraday Soc. 24, 133 (1957).

13. J. A. Pople, Proc. Roy. Soc. (London) A205, 163 (1951).

14. J. A. Pople, Proc. Roy. Soc. A202, 323 (1950).

15. J. D. Bernal and R. H. Fowler, J. Chem. Phys. 1, 515 (1933).

16. J. Lennard-Jones and J. A. Pople, Proc. Roy. Soc. (London) A205, 155 (1951).

17. T. T. Wall and D. F. Horning, J. Chem. Phys. 43, 2080 (1965).

18. D. Eisenburg and W. Kauzmann, "Structure and Properties of Water," Oxford, New York (1969).

19. I. R. Rao, Proc. Roy. Soc. (London) A130, 489 (1934).

20. P. C. Cross, J. Burnham, and P. A. Leighton, J. Am. Chem. Soc. 59, 1134 (1937).

21. D. F. Hornig, H. F. White, and F. P. Reding, Spectrochim. Acta 12, 338 (1958).

22. V. Vand and W. A. Senior, J. Chem. Phys. 43, 1878 (1965).

23. V. Vand and W. A. Senior, J. Chem. Phys. 43, 1869 (1965).

24. G. E. Walrafen, J. Chem. Phys. 47, 114 (1967).

25. W. A. Senior and V. Vand, J. Chem. Phys. 43, 1873 (1965).

26. G. E. Walrafen, J. Chem. Phys. 44, 1546 (1966).

27. N. J. Harrick, "Internal Reflectance Spectroscopy", Wiley Interscience, New York (1967).

28. G. H. Haggis, T. B. Hasted, and T. J. Buchanan, J. Chem. Phys. 20, 1452 (1952).

29. G. Nemethy and H. A. Scheraga, J. Chem. Phys. 36, 3382 (1962).

30. W. K. Thompson, W. A. Senior, and B. A. Pethica, Nature 211, 1086 (1966).

31. J. Lennard-Jones and J. A. Pople, Proc. Roy. Soc. (London) A205, 155 (1951).

32. G. Nemethy and H. A. Scheraga, J. Phys. Chem. 66, 1773 (1962).

33. M. Falk and T. A. Ford, Can. J. Chem. 44, 1699 (1966).

34. R. E. Weston, Spectrochim. Acta 18, 1257 (1962).

35. R. D. Waldron, J. Chem. Phys. 26, 809 (1957).

36. F. C. Strong, Anal. Chem. 24, 338 (1952).

37. K. Buijs and G. R. Choppin, J. Chem. Phys. 39, 2035 (1963).